# Promoting Electromagnetic Wave Absorption for Conductive Metal-Organic Framework through Crystal Morphology Controlling

*Xueling Wang, Xuan Zhang, Jiaqi Lu and Zhiliang Liu**

Inner Mongolia Key Laboratory of Chemistry and Physics of Rare Earth Materials, College of Chemistry and Chemical Engineering, Inner Mongolia University, Hohhot 010021, P. R. China.

E-mail: cezlliu@imu.edu.cn, Fax: +86-471-4992922; Tel: +86-471-4992922

## 1. Synthesis of 2,3,5,6-Tetraaminobenzoquinone (TABQ)

2,3,5,6-Tetraaminobenzoquinone (TABQ) was synthesized through a two-step coupling reaction: [1, 2]

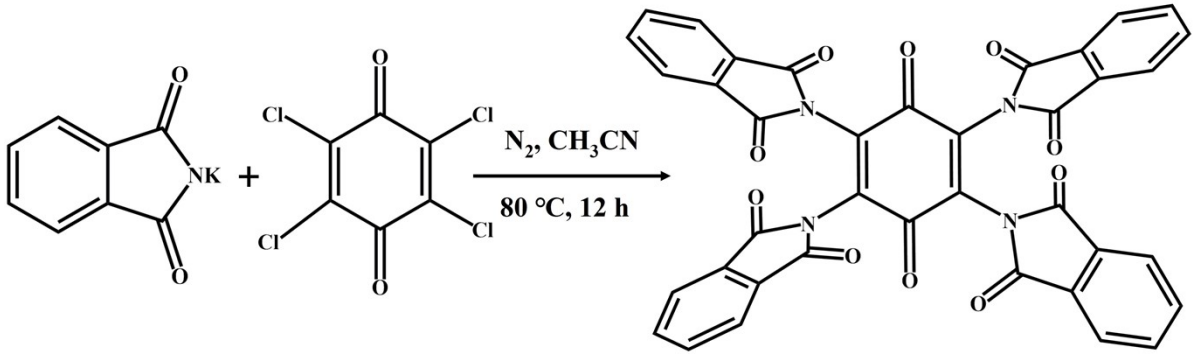


Tetrachloro-1,4-benzoquinone (20 mmol, 4.92 g) and Phthalimide potassium salt (82.30 mmol, 15.24 g) were dissolved in 80 mL acetonitrile, then reflux for 12 h under $N_2$. After cooling to room temperature, filter and collect the solid slurry, and wash first with a lot of acetonitrile, then suspend in 100 mL of DMF, heated to 100 °C, after stirring for 30 min, filter immediately while still hot. Then the obtained solids were washed several times with DMF, suspended in ethanol, heated to boiling, filtered while hot, and dried at room temperature to obtain yellow power.

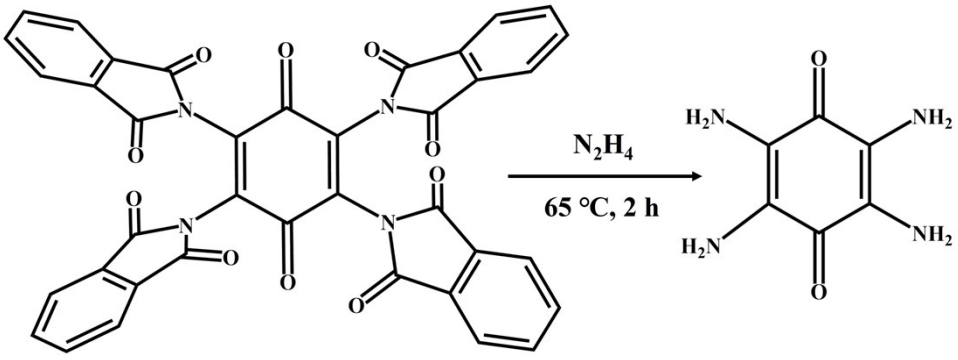


The obtained yellow powder was put into a round-bottomed flask with 75 mL hydrazine, heated to 65 ℃, stirred for 2 h, filtered under reduced pressure after cooling to room

temperature, washed with deionized water and ethanol until the filtrate was colorless, and dried overnight under vacuum at 60 ℃ to obtain purple crystalline solid (Yield: 50.60%).

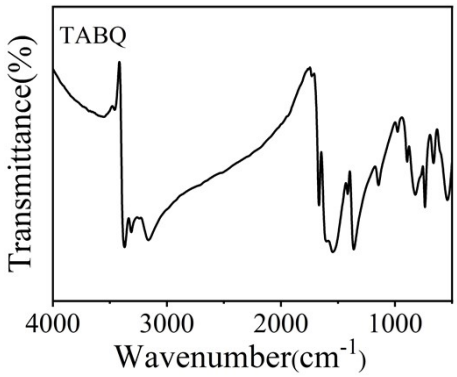


**Figure S1.** The FT-IR curves of TABQ.

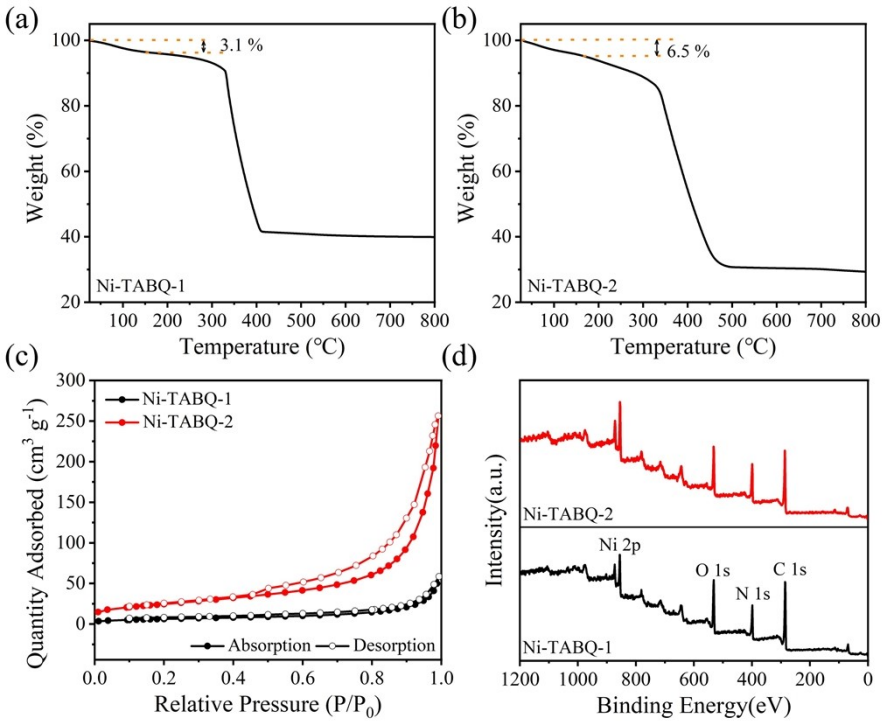


**Figure S2.** (a–b) The TG curves of Ni-TABQ-1 and Ni-TABQ-2 in the temperature range of 30-800 ℃; (c) $N_2$ adsorption−desorption isotherms, (b) XPS survey spectrum of Ni-TABQ cMOFs.

## 2. Transmission Line Theory

In general, the reflection loss value (RL) is usually used to evaluate the electromagnetic wave absorption performance of absorbers. The value can be calculated based on the transmission line theory as follows:[3]

$$Z_{in} = Z_0 \sqrt{\frac{\mu_r}{\varepsilon_r}} tanh\left[j\left(\frac{2\pi f d}{c}\right)\sqrt{\mu_r \varepsilon_r}\right] \quad (1)$$

$$RL = 20\log\left|\frac{Z_{in} - Z_0}{Z_{in} + Z_0}\right| \quad (2)$$

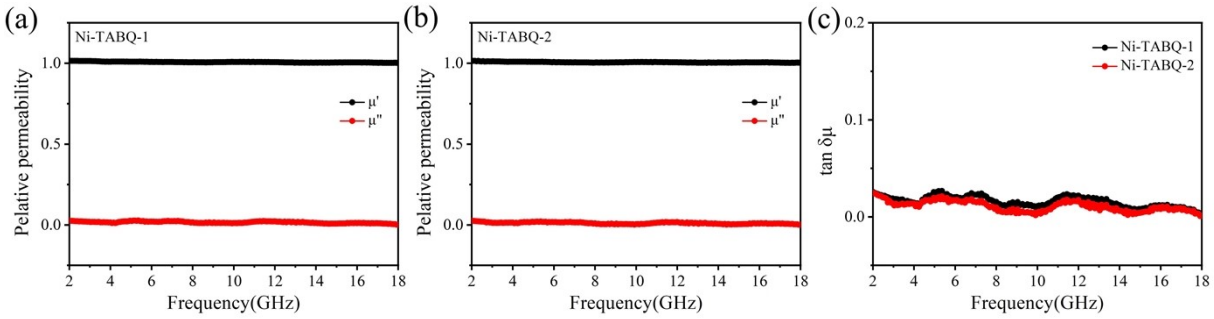


**Figure S3.** (a-b) The electromagnetic parameters and (c) the tangent value of Magnetic loss of Ni-TABQ-1 and Ni-TABQ-2.

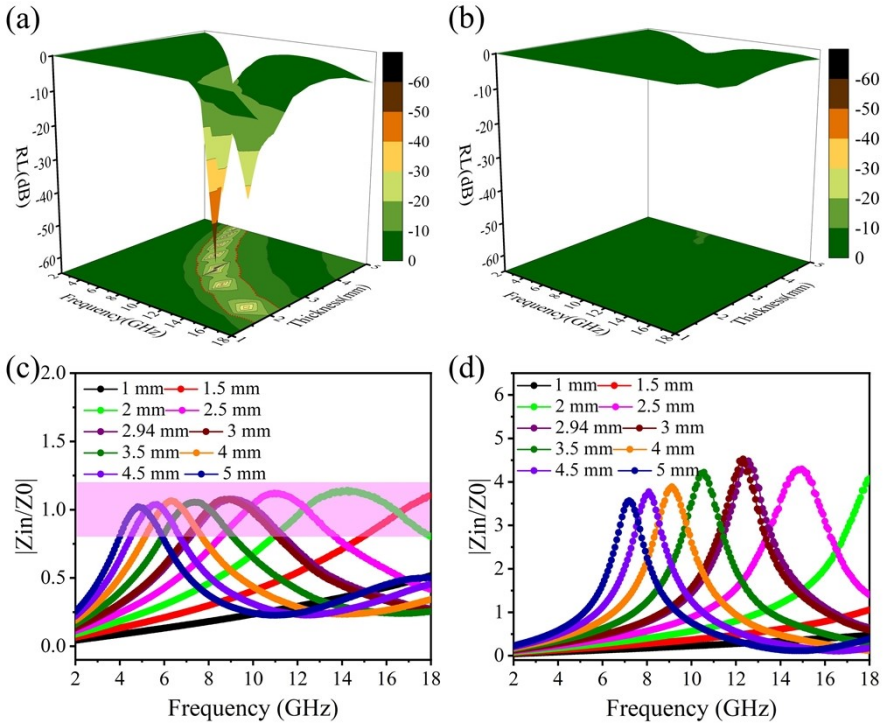


**Figure S4.** 3D RL images of (a) Ni-TABQ-1, (b) Ni-TABQ-2; and the impedance matching values of (c) Ni-TABQ-1, (d) Ni-TABQ-2.

## 3. Attenuation Constant

The attenuation constant (α) depends on the dielectric constant and permeability of absorbers, The value of α can be calculated as follows:[4]

$$\alpha = \frac{\sqrt{2}\pi f}{c} \times \sqrt{\left(\mu'' \varepsilon'' - \mu' \varepsilon'\right) + \sqrt{\left(\mu'' \varepsilon'' - \mu' \varepsilon'\right)^2 + \left(\mu' \varepsilon'' + \mu'' \varepsilon'\right)^2}} \quad (3)$$

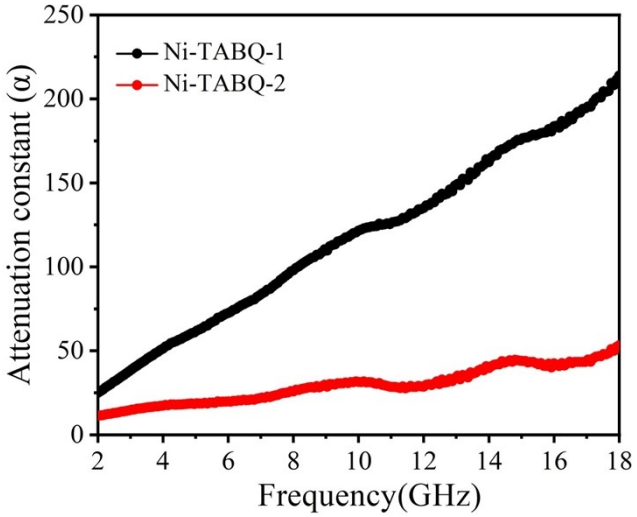


**Figure S5.** Attenuation constants value of Ni-TABQ cMOFs.

## 4. Debey Theory

According to Debye theory, dielectric loss is further divided into conduction loss ($\varepsilon_c$") and polarization loss ($\varepsilon_p$"), ε' and ε" can be expressed as follows: [5-7]

$$\varepsilon' = \varepsilon_\infty + \frac{\varepsilon_s - \varepsilon_\infty}{1 + \omega^2 \tau^2} \quad (4)$$

$$\varepsilon'' = \frac{(\varepsilon_s - \varepsilon_\infty)\omega\tau}{1 + \omega^2 \tau^2} + \frac{\sigma}{\omega \varepsilon_0} \quad (5)$$

$$\varepsilon'' = \varepsilon_p'' + \varepsilon_c'' = \frac{2\pi f \tau (\varepsilon_s - \varepsilon_\infty)}{1 + (2\pi f)^2 \tau^2} + \frac{\sigma}{2\pi f \varepsilon_0} \quad (6)$$

where $\boldsymbol{\varepsilon_s}$ and $\boldsymbol{\varepsilon_\infty}$ represent the static dielectric constant and the dielectric constant in the high-frequency limit, respectively, $\boldsymbol{\tau}$ is the relaxation time, $\boldsymbol{\omega}$ is the angular frequency of the electromagnetic wave, $\boldsymbol{\varepsilon_0}$ is the dielectric constant of free space, and $\boldsymbol{\sigma}$ is the conductivity. Equations (4) can be obtained from Equations (1) and (2) above:

$$\left(\varepsilon' - \frac{\varepsilon_s + \varepsilon_\infty}{2}\right)^2 + (\varepsilon'')^2 = \left(\frac{\varepsilon_s - \varepsilon_\infty}{2}\right)^2 \quad (7)$$

When ε' and ε" satisfy Equation (4), a semicircle in the ε' -ε" curve represents a Debye polarization relaxation process. [7, 8]

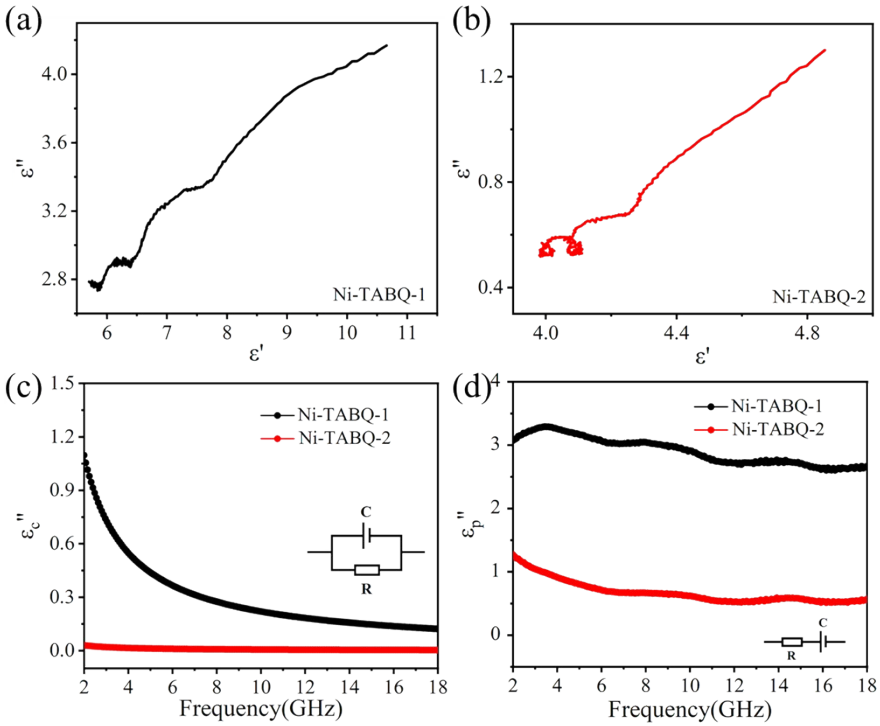


**Figure S6.** (a–b) The Cole–Cole curve, (c) conduction loss, and (d) polarization loss of Ni-TABQ cMOFs.

## 6. Quarter Wavelength (1/4λ) Matching Model

The quarter wavelength (1/4λ) matching model is used to evaluate the correlation between matching thickness and reflection loss (RL) peak frequency, which can be expressed as follows: [9, 10]

$$t_m = \frac{\lambda}{4} = \frac{nc}{4f_m\sqrt{|\varepsilon_r\mu_r|}} \text{ (n=1,3,5…)} \qquad (8)$$

Where $t_m$ is the absorber thickness, $f_m$ is the frequency at the peak $RL_{min}$, $\mu_r$ is the relative complex permeability, $\varepsilon_r$ is the relative complex permittivity, and $c$ is the speed of light in free space. That's to say, when the matched thickness satisfies the formula, the incident and reflected waves have a phase difference of 180° or odd times, and the EMW disappears at the medium/absorber interface due to the influence of interference, indicating that the absorber has efficient absorbing EMW performance.[11]

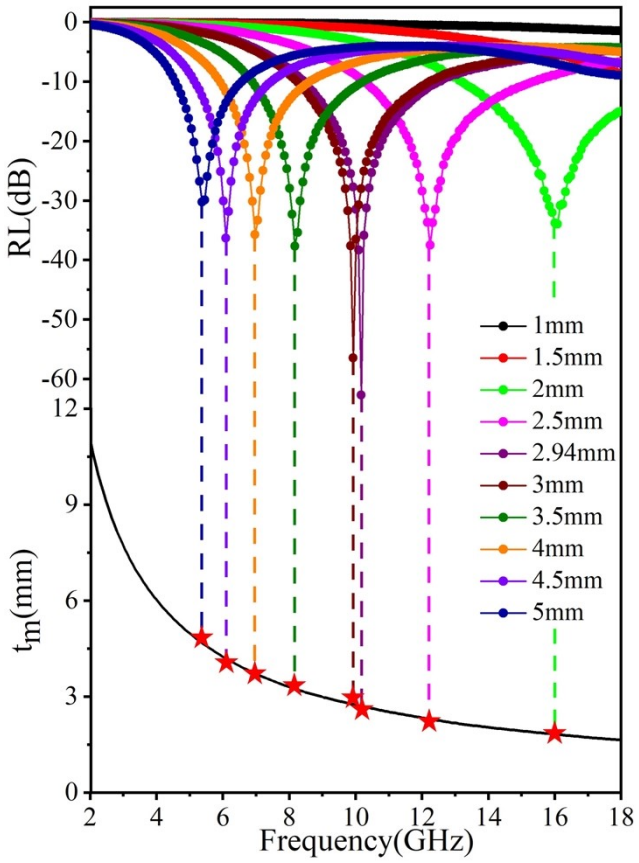


**Figure S7.** Dependence of RL on quarter-wavelength of the obtained Ni-TABQ-1.

## 7. Radar Ccross-Section (RCS) Simulation

Radar cross section (RCS) is the most critical physical indicator in radar stealth technology, which is used to evaluate the military value of materials.[12] According to the metal plate model, an absorbing coating layer with a thickness of 2.94 mm was constructed on a perfect electrical conductor (PEC) substrate of 180×180×1 $mm^3$. The incident electromagnetic wave propagates in the negative direction of the *x*-axis, and the range of pitching angle (θ) is −60°–60°, and the plane wave excitation frequency is 10.16 GHz. The RCS value was calculated as follows:[13]

$$RCS(dBm^2 = 10\log\left(\frac{4\pi S}{\lambda^2}\left|E_S/E_i\right|\right) \quad (9)$$

$\boldsymbol{S}$ is the area of the model, $\boldsymbol{\lambda}$ is the wavelength of the electromagnetic wave, $\boldsymbol{E_s}$ and $\boldsymbol{E_i}$ are the electric field intensity of the scattered and incident waves, respectively. The color of the scattered signal and the area of the radiated signal can be used to assess the intensity of the scattered signal, and the smaller the radiation area, the stronger the electromagnetic wave absorption performance.[14]

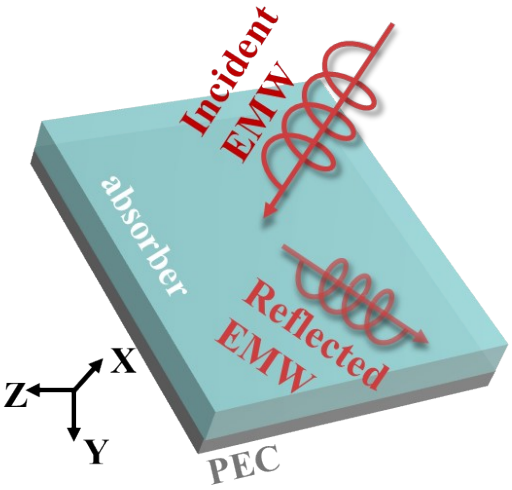


**Figure S8.** The RCS simulation model.

**Table S1.** The comparison between the optimized as-prepared Ni-TABQ-1 and conductive MOFs-based EMW absorption materials in previously reported.

| sample | Loading(wt%) | d(mm) | $RL_{min}$(dB) | EAB(GHz) | ref |
|---|---|---|---|---|---|
| Co-HHTP | 60 | 2.6 | −60.6 | 5.45 (11.89−17.34) | 15 |
| CuHT | 50 | 1.74 | −50.9 | 4.2 (7.7−10.9) | 16 |
| Cu-S-MOF | 50 | 1.69 | −52.8 | 6.72 (9.68−16.4) | 17 |
| A-Cu-HHTP | 50 | 4.4 | −51.08 | 5.73 (11.60−17.33) | 18 |
| $Zn_3Cu_1$-HHTP | 50 | 2.95 | −81.6 | 3.7 (12.5−16.2) | 19 |
| Cu-HHTP | 50 | 2.9 | −63.55 | 5.2 | 20 |
| Cu-HHTP | 40 | 2.1 | −43.5 | 5.76 | 21 |
| CuNi-3/ACET | 40 | 3.5 | −40.54 | 5.87 | 22 |
| Cu-DCNQI | 20 | 0.9 | −33.2 | 2.7 | 23 |
| $Cu_{1.3}Ni_{1.7}(HITP)_2$ | 15 | 2.1 | −71.5 | 6.16 (11.84−18) | 24 |
| $Co_{0.5}Cu_{0.5}$−CAT−1 | | 2.26 | −61.0 | 6.16 | 25 |
| iron-quinoid MOF-160 | 30 | 3.3 | −73.5 | 6.1 (9.8−15.9) | 26 |
| **Ni-TABQ-1** | **40** | **2.94** | **−62.68** | **5.12 (10.24−15.36)** | **This work** |

**Reference**


1. Z. Lin, H.-Y. Shi, L. Lin, X. Yang, W. Wu and X. Sun, *Nat. Commun.*, 2021, **12**, 4424.
2. Z. Luo, L. Liu, J. Ning, K. Lei, Y. Lu, F. Li and J. Chen, *Angew. Chem. Int. Ed.*, 2018, **57**, 9443-9446.
3. X. Zeng, X. Cheng, R. Yu and G. D. Stucky, *Carbon*, 2020, **168**, 606-623.
4. X. Chen, X. Wang, K. Wen, J. Zhang, F. Zhao, J. Zhang, Y. Wang, Q. Song, C. Yi and J. Shao, *Carbon*, 2023, **203**, 706-716.
5. M. S. Cao, X. X. Wang, M. Zhang, J. C. Shu, W. Q. Cao, H. J. Yang, X. Y. Fang and J. Yuan, *Adv. Funct. Mater.*, 2019, **29**, 1807398.
6. Q. Wang, B. Niu, Y. Han, Q. Zheng, L. Li and M. Cao, *Chem. Eng. J.*, 2023, **452**, 139042.
7. B. Quan, X. Liang, G. Ji, Y. Cheng, W. Liu, J. Ma, Y. Zhang, D. Li and G. Xu, *J. Alloys Compd.*, 2017, **728**, 1065-1075.
8. Y. Zhang, X. Liu, Z. Guo, C. Jia, F. Lu, Z. Jia and G. Wu, *J. Mater. Sci. Technol.*, 2024, **176**, 167-175.
9. Y. Ma, Y. Jiang, J. Qian, C. Wang, S. Kang, G. Chen and B. Zhong, *Ceram. Int.*, 2023, **49**, 18745-18755.
10. Z. Qin, C. Wang, Y. Ma, L. xia, B. Zhong, X. Li and P. Zhang, *Appl. Surf. Sci.*, 2022, **575**, 151789.
11. X. Xu, Y. Wang, Y. Yue, C. Wang, Y. Wang and D. Liu, *Compos. Part A-Appl. S.*, 2022, **162**, 107138.
12. L. Xing, H. Cheng, Y. Li, Q. Chen and X. Liu, *Chem. Eng. J.*, 2024, **487**, 150729.
13. S. Xu, P. Liao, J. Zhu, Z. Yao, X. Zhang, J. Yuan, C. Rong, X. Liu, Z. Xiong and F. Kuang, *Appl. Surf. Sci.*, 2024, **649**, 159200.
14. W. Deng, T. Li, H. Li, J. abdul, L. Liu, A. Dang, X. Liu, M. Duan and H. Wu, *Small*, 2024, **n/a**, 2309806.
15. A. Dong, Z. Mu, X. Meng, S. Li, J. Li, L. Dai, J. Lv, P. Li and B. Wang, *Chem. Eng. J.*, 2022, **444**, 136574.
16. P. Miao, T. Zhang, T. Wang, J. Chen, T. Gao, Y. Wang, J. Kong and K.-J. Chen, *Chin. J. Chem* . 2022, **40**, 467-474.
17. P. Miao, N. Qu, W. Chen, T. Wang, W. Zhao and J. Kong, *Chem. Eng. J.*, 2023, **454**,

140445.

18. X. Wang, X. Zhang, A. He, J. Guo and Z. Liu, *Inorg. Chem.*, 2024, **63**, 6948-6956.
19. X. Zhang, X. Tian, N. Wu, S. Zhao, Y. Qin, F. Pan, S. Yue, X. Ma, J. Qiao, W. Xu, W. Liu, J. Liu, M. Zhao, K. Ostrikov and Z. Zeng, *Sci. Adv.*, 2024, **10**, eadl6498.
20. X. Zhang, X.-L. Tian, Y. Qin, J. Qiao, F. Pan, N. Wu, C. Wang, S. Zhao, W. Liu, J. Cui, Z. Qian, M. Zhao, J. Liu and Z. Zeng, *ACS Nano*, 2023, **17**, 12510-12518.
21. Z. Shan, S. Cheng, F. Wu, X. Pan, W. Li, W. Dong, A. Xie and G. Zhang, *Chem. Eng. J.*, 2022, **446**, 137409.
22. J. Cheng, H. Zhang, H. Wang, Z. Huang, H. Raza, C. Hou, G. Zheng, D. Zhang, Q. Zheng and R. Che, *Adv. Funct. Mater.*, 2022, **32**, 2201129.
23. L. Wu, A. Xie, F. Wu, J. Shi, Q. Sun and W. Dong, *Adv. Mater. Interfaces*, 2021, **8**, 2100712.
24. C. Chen, Z. Shan, S. Tao, A. Xie, H. Yang, J. Su, S. Horke, S. Kitagawa and G. Zhang, *Adv. Funct. Mater.*, 2023, **33**, 2305082.
25. N. Qu, G. Xu, Y. Liu, M. He, R. Xing, J. Gu and J. Kong, *Adv. Funct. Mater.*, 2024, **n/a**, 2402923.
26. H. Wei, Y. Tian, Q. Chen, D. Estevez, P. Xu, H.-X. Peng and F. Qin, *Chem. Eng. J.*, 2021, **405**, 126637.